ACS Sustainable Chemistry & Engineering

Research Article

pubs.acs.org/journal/ascecg

Novel and High-Performance Magnetic Carbon Composite Prepared from Waste Hydrochar for Dye Removal

Xiangdong Zhu, Yuchen Liu, Chao Zhou, Shicheng Zhang,* and Jianmin Chen

Shanghai Key Laboratory of Atmospheric Particle Pollution and Prevention (*LAP*^{3}), Department of Environmental Science and Engineering, Fudan University, Shanghai 200433, China

Supporting Information

ABSTRACT: In recent years, more and more attention has been paid to the hydrothermal liquefaction (HTL) of waste biomass for the production of bio-oil and hydrochar (a solid residue from HTL process). However, hydrochar possesses limited porosity and surface area, hindering its environmental application. In the present work, to promote the development of a sustainable application of waste biomass, waste hydrochar was activated and modified to a novel magnetic carbon composite, which exhibited high performance for dye removal from aqueous solutions. The composite possessed a saturation magnetization of 38.5 emu g^{-1} at room temperature and could be facilely attracted from an aqueous solution by an external magnet. The as-prepared composite exhibited a superior malachite green (MG) adsorption capacity (476 mg g^{-1}), which was much higher than the known magnetic adsorbents. Our results suggested that the waste hydrochar could be efficiently transformed to a high-performance sustainable material for dye removal.

KEYWORDS: *Hydrochar, Magnetic carbon composite, Malachite green, Adsorption*

INTRODUCTION

In the past few years, hydrothermal liquefaction (HTL) of biomass has received much attention due to the growing environmental and energy crisis.[1] HTL is a thermal chemical conversion process showing a tremendous advantage for the transformation of wet biomass into valuable products, such as bio-oil and hydrochar.[2−6] The hydrochar is composed of spherical microparticles with a low level of aromatic and high degree of oxygen-contained functional groups, which allow this material to be suitable as a template for the fabrication of metal/carbon composites.[7] It is an attractive material that has been revealed as an efficient adsorbent for pollutants removal.[8,9] However, one shortcoming of hydrochar is its limited porosity and surface area,[10] which hinders its wide application in the field of environmental remediation unless it is subjected to chemical or physical activation.[7,11] Hence, the synthesis of high-performance carbon composites derived from hydrochar presents a challenge.

Hydrochar activated by potassium hydroxide (KOH) has been previously investigated, and the resultant products have narrow micropore-sized distributions and high surface areas.[7,12] However, KOH is a deleterious substance. Waste carbonaceous material activated by potassium carbonate (K_2CO_3) also can prepare activated carbon with high surface area.[13] K_2CO_3 is not deleterious as used for food additives. There has been few reports on activation of hydrochar by K_2CO_3. Nevertheless, the spent adsorbents often contain a great number of pollutants, which may generate the risk of secondary contamination. Generally, introducing magnetite or maghemite (magnetic medium) to waste biomass, commercial-activated carbon, or carbon nanotubes via hydrothermal coprecipitation of ferrous and ferric ions under basic solution is a facile method to enable the carbonaceous material to be rapidly separated from aqueous solutions by an external magnet. However, only the magnetic carbon composite prepared from activated carbon retains abundant pore structure and large surface area for removal of pollutants due to the negative effect of the magnetic medium.[14−16] Hence, to obtain a high-performance magnetic carbon composite, the activation conditions of waste hydrochar should be optimized first. Although there are many researchers focused on the activation and modification of waste biomass for

Received: December 21, 2013
Revised: January 22, 2014
Published: January 29, 2014

Table 1. Textural Properties of Activated Carbon Prepared under Different Conditions

temperature (°C)	impregnation ratio	yield (%)	S_{BET} [a] ($m^2\ g^{-1}$)	S_{mic} [b] ($m^2\ g^{-1}$)	S_{mic}/S_{BET} (%)	V_T [c] ($cm^3\ g^{-1}$)	V_{mic} [d] ($cm^3\ g^{-1}$)	V_{mic}/V_T (%)
600	0.5	44.7	742.9	694.4	93.5	0.483	0.347	71.8
600	1	40.0	771	710.9	92.2	0.503	0.356	70.8
600	2	47.3	636.3	583.4	91.7	0.415	0.292	70.4
600	4	44.7	658.5	620.6	94.2	0.425	0.311	73.2
500	2	49.8	444.5	400.2	90.0	0.307	0.200	65.1
700	2	32.8	1037	956.8	92.3	0.600	0.474	79.0
800	2	23.7	1541	1393	90.4	0.943	0.693	73.5

[a]Measured using N_2 adsorption with the Brunauer–Emmett–Teller (BET) method. [b]Micropore surface area calculated using the *t*-plot method. [c]Total pore volume determined at $P/P_0 = 0.99$. [d]Micropore volume calculated using the *t*-plot method.

environmental application, to the best of our knowledge, this type of material has not been used previously to prepare a magnetic carbon composite.[1,7−9]

Because triphenylmethane dye (i.e., malachite green, MG) is relatively inexpensive and effective, it has been used widely in the field of dyeing of textiles, fungicides, and antiseptics. Because of its toxicity, carcinogenicity, and mutagenic and teratogenic properties, MG contamination has become a great environmental concern with potential adverse effects to human health.[14,17] Therefore, it is necessary to remove them from wastewater before the wastewater is discharged into bodies of water. Adsorption is an effective means to reduce the concentration of the contaminant with lower operation cost. However, the known magnetic adsorbent often exhibited low adsorption capacity for MG removal due to its poor pore volume.[14]

In the present study, the hydrochar was selected as a carbon precursor to prepare a novel and high-performance magnetic carbon composite. In order to obtain a high-performance magnetic carbon composite, the preparation conditions of activated carbon are first optimized. The main objectives of this research are to investigate the characteristics of a magnetic carbon composite derived from waste hydrochar and to estimate the adsorption ability of the magnetic carbon composite for MG removal.

EXPERIMENTAL SECTION

Materials. The MG and humic acid (HA) was obtained from Aladdin Reagent Co. Ltd., China. Other reagents (analytical grade) were purchased from Sinopharm Chemical Reagent Co. Ltd., China. Ultrapure water was collected from a Milli-Q academic water purification system. The hydrochar material was a solid residual of HTL of *Salix psammophila* (SP), obtained from our pilot-scale HTL unit. A more detailed procedure for preparation of hydrochar is available in the Supporting Information.

Preparation of Magnetic Carbon Composite. The synthesis methodology of the magnetic carbon composite was comprised of two steps: (1) preparation of activated carbon via chemical activation of hydrochar by K_2CO_3 and (2) preparation of the magnetic carbon composite via the precipitation of iron oxides onto the activated carbon.[13,18] The schematic illustration of the preparation of the activated carbon and magnetic carbon composite is depicted in Figure S1 of the Supporting Information. A more detailed process for the synthesis of the activated carbon and magnetic carbon composite is presented in the Supporting Information.

Characterization of Samples. The Brunauer–Emmett–Teller (BET) surface area of the samples was performed by nitrogen (N_2) adsorption at −196 °C using a Quantasorb SI instrument (Quantachrone, U.S.A.). The microscopy measurements of the sample were performed using transmission electron microscopy (TEM, 75 Kv, Hitachi, H-600) and scanning electron microscopy/energy dispersive X-ray spectrometry (SEM/EDX, XL300, Link 300, Philips). The saturation magnetization of the sample was determined with a vibrating sample magnetometer (VSM, quantum) at 300 K. The X-ray diffraction (XRD) pattern of the sample was collected by a X-ray diffractometer with a copper (Cu) monochromator (40 Kv, 40 mA). The scan was run from 20° to 80° with a step size of 0.05°.

Fourier transform-infrared (FT-IR) studies were done with a Nicolet (Nexus 470) spectrometer in wavenumber ranges of 4000–400 cm^{-1}. The Raman spectroscopy was recorded using a LabRam-1B spectrometer. The X-ray photoelectron spectroscopy (XPS) was performed by a RBD upgraded PHI-5000C ESCA system (Perkin-Elmer) with Mg Kα radiation ($h\nu$ = 1253.6 eV). Binding energies were calibrated by setting C to 1s at 284.6 eV. In addition, a detailed procedure for determination of zero point charges (pH_{PZC}) of the composite is also available in the Supporting Information.[19]

Batch Adsorption Experiments. The adsorption experiments were performed in 120 mL glass bottles with 0.04 g of the magnetic carbon composite and 80 mL of the MG solution on a shaker at 25 °C. The pH of solution was adjusted with NaOH or HCl (0.1 M). An operational background solution containing different concentrations of HA was also used as needed. Samples were withdrawn and subjected to filtration through a 0.22 μm membrane filter. The adsorption experiments were performed in duplicate.

The concentrations of the MG were measured by a UV–vis spectrophotometer (TU-1900, Pgeneral Co. Ltd., Beijing) at 620 nm. The adsorbed amounts of MG at equilibrium (q_e, mg g^{-1}) were calculated using the following equation (eq 1)

$$q_e = \frac{(C_0 - C_e)V}{m} \quad (1)$$

where C_0 and C_e are the initial and equilibrium concentrations of MG (mg L^{-1}), respectively; m is the mass of the composite (g); and V is the volume of reaction solution (L).[20,21]

RESULTS AND DISCUSSION

Investigations of Activation Conditions. The porosity development of activated carbon is greatly affected by the activation conditions, such as activation temperature and the impregnation ratio of the activator. As a result, the effect of the activation conditions (impregnation ratio of K_2CO_3 and temperature) upon the porosity of resultant products was first established. The N_2 adsorption–desorption isotherms of the resultant activated carbon under various activation conditions are shown in Figures S2 and S3 of the Supporting Information. All of the adsorption isotherms of the products, regardless of the activation conditions, showed type I isotherms, suggesting the existence of large fractions of micropores.[22] Table 1 shows the textural characteristics of products prepared under various conditions. The influence of the impregnation ratio of K_2CO_3 on pore volume and BET surface area was not so obvious, which indicated that textural characteristics of products were less sensitive to the impregnation ratio.

Table 2. Textural Properties of Hydrochar, Activated Carbon, and Composite Samples

sample	S_{BET} [a] ($m^2\ g^{-1}$)	S_{mic} [b] ($m^2\ g^{-1}$)	S_{mic}/S_{BET} (%)	V_T [c] ($cm^3\ g^{-1}$)	V_{mic} [d] ($cm^3\ g^{-1}$)	V_{mic}/V_T (%)
hydrochar	6.86	–	0	0.041	–	0
activated carbon	1230	1106	89.9	0.810	0.548	67.7
composite	673	566	84.1	0.646	0.281	43.5

[a]Measured using N_2 adsorption with the Brunauer–Emmett–Teller (BET) method. [b]Micropore surface area calculated using the *t*-plot method. [c]Total pore volume determined at P/P_0 = 0.99. [d]Micropore volume calculated using the *t*-plot method.

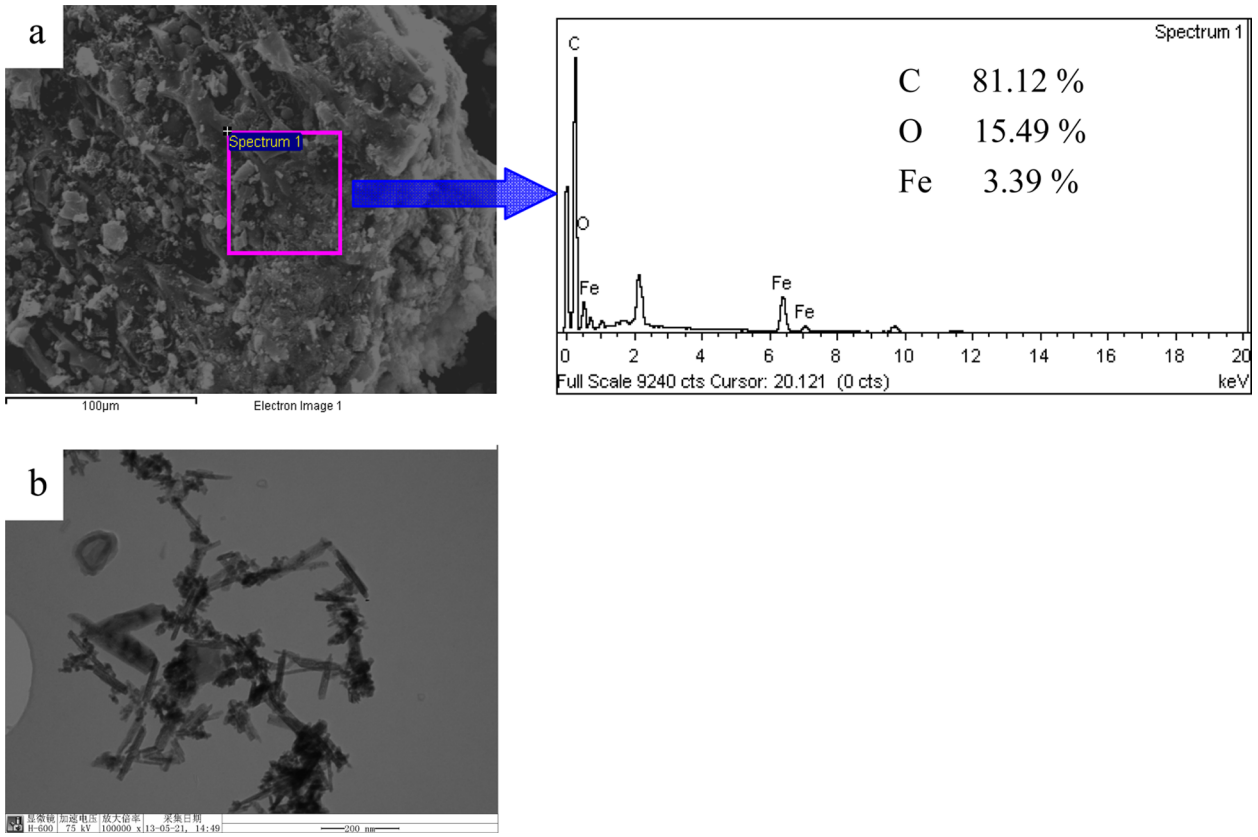

Figure 1. SEM/EDX spectra for the composite (a) and TEM image of the composite (b).

Apparently, the N_2 uptakes were significantly increased with increasing activation temperature (Figure S3, Supporting Information). Accordingly, development of BET surface area, total pore volume, and micropore volume with activation temperature was observed. However, the proportion of micropore volume gradually increased before 700 °C and then slightly decreased at higher temperature (800 °C), which can be attributed to the widening of the existing pores by the heat effect.[23] Hence, the phenomenon of overgasification occurred and decreased the microporosity beyond 700 °C.

Characterization of Samples. The activated sample derived from 700 °C and a 2:1 impregnation ratio was used to prepare the magnetic carbon composite. As shown in Table 2, the hydrochar showed extremely low surface area (6.86 $m^2\ g^{-1}$). The surface of the hydrochar was covered by untransferred organic matter and migrated compounds from the liquid phase, which may reduce the porosity of the hydrochar.[24] After activation and magnetization, the porous textural characteristics of the activated carbon and magnetic composite were also studied. As shown in Figure S4 of the Supporting Information, the N_2 adsorption isotherms of the products were typical type I isotherms, denoting microporous solids. The textural properties of the samples are also shown in Table 2.

It was found that 19.8% and 49.1% of the total pore volume and micropore volume, respectively, of the activated carbon were diminished after precipitation of iron oxides or hydroxides due to the covering of the surface of the activated carbon by the magnetic medium. However, the magnetic carbon composite still retained a high surface area and pore volume for the filling of pollutants.

The technology of magnetic separation exhibited tremendous potential for superior separation efficiency, which greatly enhanced the recycling potential of the magnetic composite.[25] The magnetic property of the composite is studied by VSM. Figure S5 of the Supporting Information shows the hysteresis loop between ±20 kOe at 300 K, with the composite having a saturation magnetization of 38.5 emu g^{-1} and exhibiting a superparamagnetic characteristic.[26] The insert in Figure S5 of the Supporting Information shows that the particles of the prepared magnetic composite could be facilely attracted by an external magnet, which indicated that this composite could be used as a magnetic material to remove containments from aqueous solution.

dx.doi.org/10.1021/sc400547y | ACS Sustainable Chem. Eng. 2014, 2, 969–977

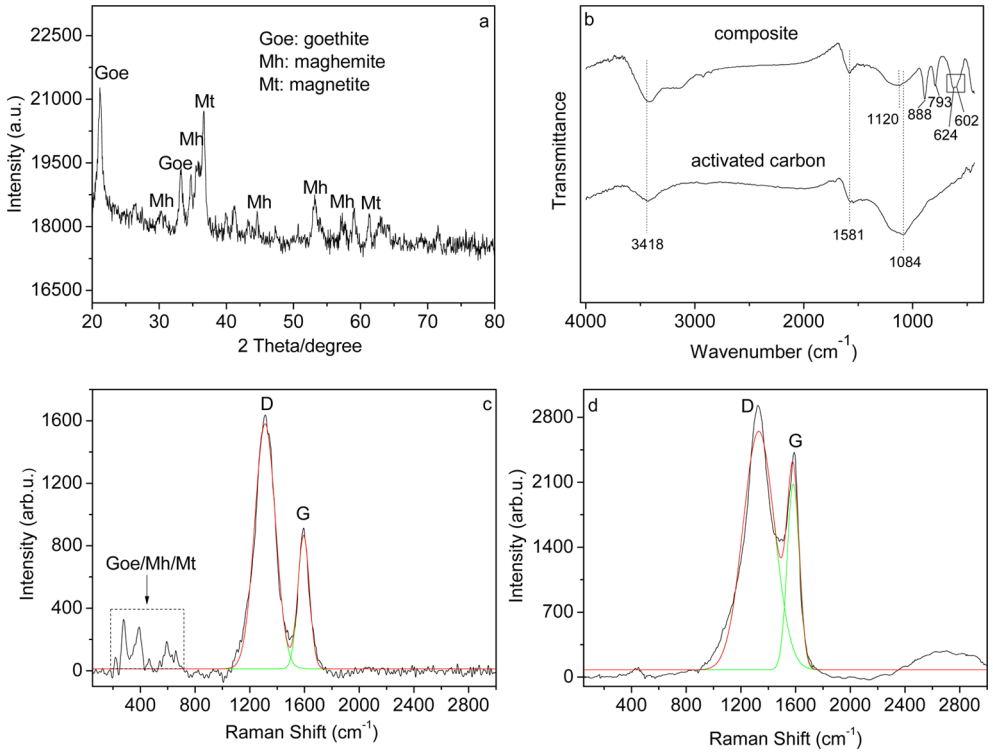

Figure 2. (a) Power X-ray diffraction (XRD) pattern for the composite, (b) FT-IR spectra of the composite and activated carbon, (c) Raman spectra of the composite, and (d) Raman spectra of activated carbon (green line, integral peak; red line, fitted curve by Guassian type).

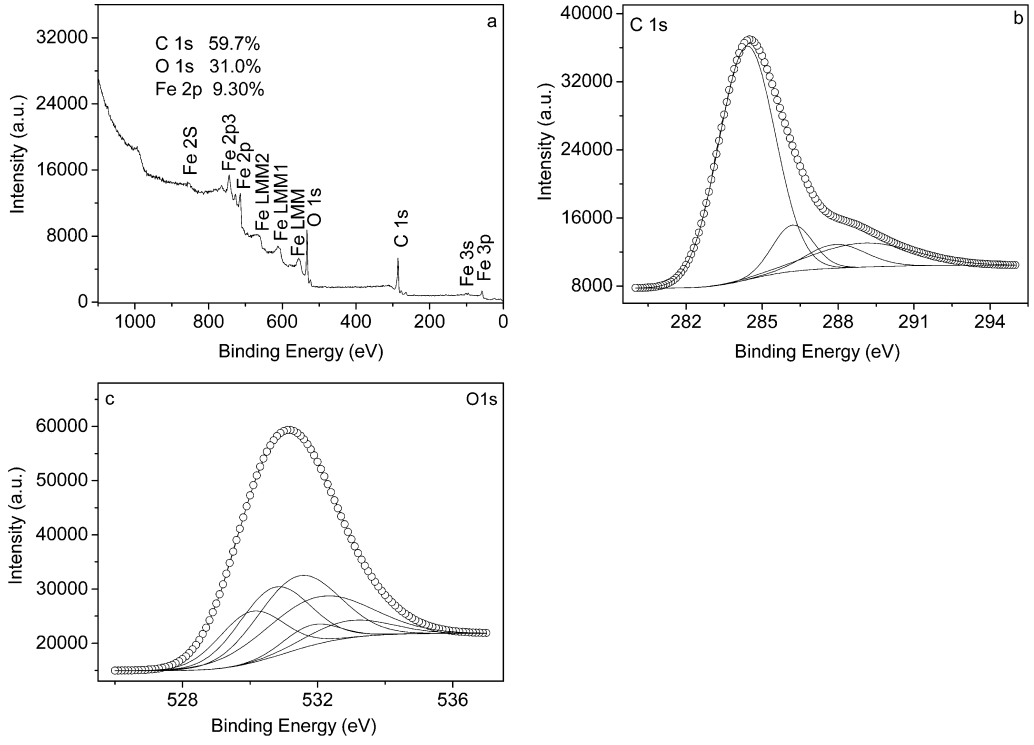

Figure 3. (a) X-ray photoelectron spectroscopy (XPS) spectra: wide scan, (b) Fe 2p spectra, C 1s high-resolution spectra of the composite, and (c) O 1s high-resolution spectra of the composite.

The morphology of the composite was studied through SEM/EDX and TEM observations (Figure 1). The surface of the activated carbon was covered by iron oxide or hydroxide particles, as indicated by the morphology of the composite. The element composition of the composite was summarized with EDX technology. It was clear that the composite contained carbon, oxygen, and iron, with the main carbon element. As shown in Figure 1b, the primary particles of the composite exhibited needle-like and bulk shapes; in addition, the average length of the particles was about 200 nm. The light-colored

dx.doi.org/10.1021/sc400547y | ACS Sustainable Chem. Eng. 2014, 2, 969−977

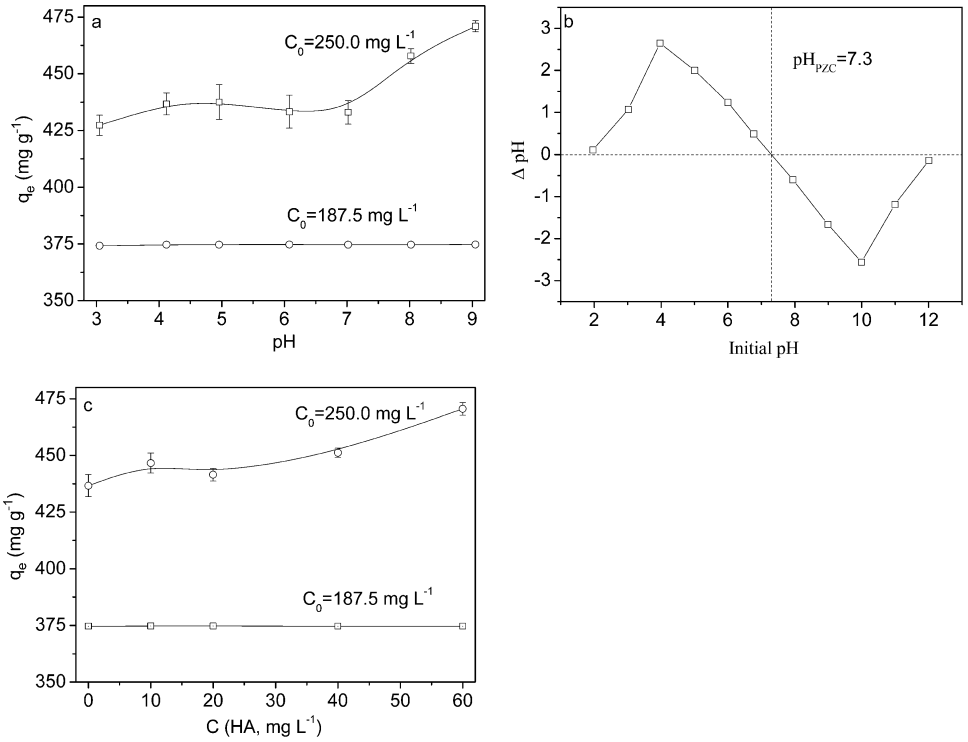

Figure 4. (a) Effect of solution pH on the equilibrium uptake of MG. Reaction conditions: contact time, 12 h; temperature, 25 °C; and composite, 500 mg L^{-1}. (b) pH_{PZC} of composite sample. (c) Effect of HA on the equilibrium uptake of MG. Reaction conditions: solution pH, 4.3; contact time, 12 h; temperature, 25 °C; and composite, 500 mg L^{-1}.

region showed the presence of the carbon matrix (Figure 1b); however, the black region was iron particles due to the difference of electron penetrability.[14] The well-dispersed iron oxide or hydroxide particles within the pores of the activated carbon matrix was observed, which prevented the separation of the iron particles from the activated carbon matrix under the action of external forces.[27]

The XRD analysis of the composite displayed a number of peaks (2θ = 21.2°, 30.2°, 33.2°, 35.6°, 36.7°, 44.7°, 53.1°, 57.4° and 61.3°) (Figure 2a). These peaks were assigned to maghemite (peaks at 2θ = 30.2°, 35.6°, 44.7°, 53.1°, and 57.4°), magnetite (peaks at 2θ = 36.7 and 61.3°), and goethite (peaks at 2θ = 21.2 and 33.2°).[18,28] This illustrated that the domain of the iron species resulted from the process of adsorption, hydrolysis, and precipitation.[28]

As shown in Figure 2b, the functional groups of the surface of the composite and activated carbon were studied. The composite and activated carbon displayed the same adsorption bands at 3418, 1581, and 1180/1084 cm^{-1} assigned to O−H, aromatic C−C, and C−O bonds stretch, respectively.[29,30] The composite exhibited two additional bands around 624 and 602 cm^{-1}, as the indication of maghemite and magnetite, respectively.[31] However, the new bands at 888 and 793 cm^{-1} corresponded to O−H vibrations in plane and out of plane, respectively, which were the indicator of goethite.[32] The same results were observed with the XRD analysis. These oxygen-containing functional groups may react with the MG molecule by means of specific adsorption such as H-bonding and $\pi-\pi$ interaction, which may enhance MG adsorption efficiency.[29]

The structure of the carbon phase and iron oxides of the composite and activated carbon were also studied by Raman spectroscopy (Figure 2c, d). Compared with Figure 2d, Figure 2c exhibited the additional peaks over the wavelength from 200 to 800 cm^{-1}, which was attributed to maghemite, magnetite, and goethite.[33,34] The characteristic peak of magnetite was observed at 663 cm^{-1}. The other two intensity bands located at around 1320 and 1580 cm^{-1} were assigned to the defect sp^3 carbon band (D band) and stretching vibrations of basal graphite layers (G band), respectively.[35] The ratio of the G/D bands (indicator of sample crystallinity) of both the composite and activated carbon were all found to be 0.30, which indicated that graphitic layers of the samples were semicrystalline and possessed defects.[36]

As shown in Figure 3a, the wide scan XPS spectra of the magnetic composite showed the presence of C 1s, O 1s, and Fe 2p. The carbon/oxygen/iron atomic ratio was 6.4:3.3:1. Deconvolution of the C 1s and O 1s peaks of the composite indicated the presence of different functional groups (Figure 3b, c). The relative peak areas of C and O in different forms on the surface of the composite are listed in Table S1 of the Supporting Information.[29,30] It was evident that the main functional groups containing C and O were C−C (284.4 eV) and C−O−C (531.4 eV), respectively. In addition, the composition ratio of maghemite, magnetite, and goethite was 4.4: 4.4: 1, which was concluded from the peak area of the deconvolution of the O 1s.

Effect of Solution pH on MG Adsorption. Both aqueous chemistry and the surface binding sites of an adsorbent were influenced by solution pH. Hence, the effect of solution pH on MG adsorption was studied in the pH value range of 3−9. As shown in Figure 4a, the adsorption capacity of MG by the composite was relatively low at acidic conditions, and the maximum was obtained at pH 9, with the initial MG concentration of 250.0 mg L^{-1}.

The MG molecule has high positive charge density at lower pH, which results from protonation in the acidic medium and

dx.doi.org/10.1021/sc400547y | ACS Sustainable Chem. Eng. 2014, 2, 969−977

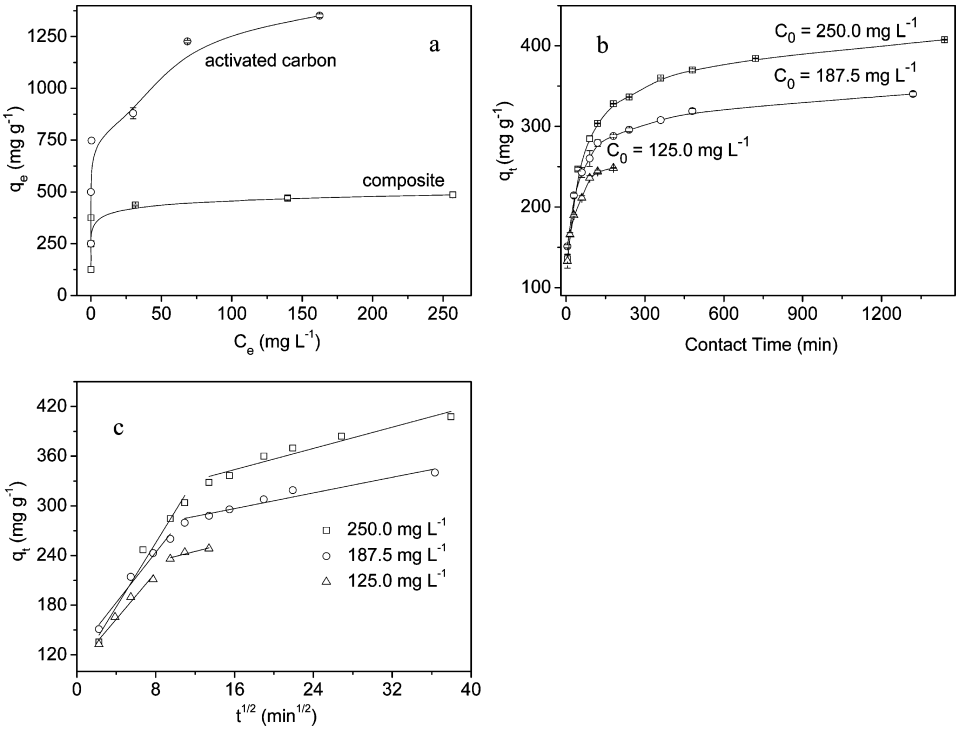

Figure 5. (a) Adsorption isotherm of MG on the composite and activated carbon. Reaction conditions: natural solution pH; contact time, 24 h; temperature, 25 °C; and composite, 500 mg L^{-1}. (b) Effect of contact time on the adsorption of MG with different initial MG concentrations. Reaction condition: natural solution pH; temperature, 25 °C; and composite, 500 mg L^{-1}. (c) Intraparticle diffusion plot for the MG adsorption with different initial concentrations at 25 °C.

Table 3. Comparisons of MG Maximum Adsorption Capacity (q_{max}, mg g^{-1}) of Carbon Adsorbents

adsorbents	carbon source	activator	q_{max}	reference
activated carbon/$CoFe_2O_4$ composite	commercial	–	~ 81	14
activated carbon	rice husk	H_3PO_4, NaOH	~ 90	17
activated carbon	bamboo	K_2CO_3	~ 242	41
bioadsorbent	*Zea mays* husk leaf	$Ca(OH)_2$	~ 72	42
ordered mesoporous carbon	furfuryl alcohol	oxalic acid	354.5	43
activated carbon	hydrochar of SP	K_2CO_3	1354	this study
activated carbon/iron oxide	hydrochar of SP	K_2CO_3	486	this study

deprotonation at higher pH (pK_a = 10.3). As shown in Figure 4b, at lower pH values, a positive surface charge could be formed from the protonation of π electron-rich regions on the surface of the composite. Hence, the electrostatic repulsion may reduce the uptake of the positive-charged MG molecule. When solution pH increased, the oxygen-containing groups were ionized, and the negative charge density on the surface increased. This could enhance the adsorption efficiency of MG through the electrostatic force of attraction.[26]

However, when the initial MG concentration was decreased to 187.5 mg L^{-1} (removal efficiency of MG was 100%), the effect of pH on MG adsorption was negligible because the composite may not have reached the maximum adsorption capacity.

Effect of Humic Acid on MG Adsorption. HA was selected as the model natural organic matter (NOM) to evaluate the effect of NOM on MG adsorption because 70% of NOM is composed of HA.[37] As shown in Figure 4c, when the initial MG concentration was 187.5 mg L^{-1}, the effect of HA on MG adsorption was not observed (removal efficiency of MG was 100%) because the MG molecules in aqueous solution were all adsorbed by the composite due to its having enough pores for the filling of MG. Hence, the effect of HA on MG adsorption is invisible under such an initial MG concentration.

When the initial MG concentration was increased to 250.0 mg L^{-1}, an increase in the MG adsorption was observed because the magnetic composite has not reached the maximum adsorption capacity. Interestingly, HA showed a slightly increased effect (rather than a suppressing effect) on MG adsorption, which may be ascribed to the following factors: First, the MG molecule may have a strong adsorption affinity toward the composite and thus could compete with the HA molecule for the adsorption sites.[38] Second, the adsorbed HA molecule may provide some sorption site to the MG molecule, which induces slightly enhanced MG adsorption with increased HA concentration.[39] Hence, the effect of the solution conditions (such as solution pH and HA concentration) on MG adsorption by the prepared magnetic composite was influenced by the MG initial concentration.

Adsorption Isotherms. As shown in Figure 5a, the adsorption capacity of MG by the composite increased with increasing MG concentration. In contrast, the adsorption process of MG on the activated carbon was also studied. It was evident that the adsorption capacity of MG on the activated

Table 4. Kinetics Model Parameters for Adsorption of MG onto the Composite at 25 °C[a]

pseudo-first-order model					pseudo-second-order model				Elovich		
C_0	q_{exp}	q_e	k_1	R^2	q_e	k_2	h	R^2	α	β	R^2
125.0	248	138	0.027	0.98	256	5.25×10^{-7}	0.0345	0.99	311	0.029	0.98
187.5	340	130	0.0041	0.91	345	6.86×10^{-7}	0.0816	0.99	588	0.028	0.98
250.0	407	173	0.0031	0.91	417	5.85×10^{-7}	0.102	0.99	175	0.020	0.99

[a] C_0, mg L^{-1}; q_{exp}, mg g^{-1}; q_e, mg g^{-1}; k_1, min^{-1}; k_2, g mg^{-1} min^{-1}; h, mg g^{-1} min^{-1}; α, mg g^{-1} min^{-1}; and β, g mg^{-1}.

carbon was significantly more than on the magnetic composite, indicating that MG removal mainly resulted from those carbonized materials rather than the magnetic iron oxide.

The shape of the adsorption isotherm of MG on the composite was defined as L-behavior based on the Giles' classification,[40] and the adsorption process of MG on the composite was fitted with the linear form of the Langmuir model. The Langmuir model is expressed as

$$\frac{C_e}{q_e} = \frac{1}{bq_m} + \frac{C_e}{q_m} \tag{2}$$

where the values of b (L mg^{-1}) and q_m (mg g^{-1}) represent the Langmuir isotherm coefficients and monolayer adsorption capacity, respectively.

The fitted Langmuir isotherm was found to be linear (R^2 = 0.99). The value of q_m for the adsorption of MG was 476 mg g^{-1}, which was in accordance with the obtained experimental value of 486 mg g^{-1}. When compared with previously reported adsorbents (Table 3),[14,17,41−43] this result indicated that the magnetic carbon composite prepared from hydrochar of SP has great potential as an adsorbent for MG removal.

For the Langmuir adsorption, to estimate if the adsorption process was favorable or unfavorable, the isotherm can be classified by the separation factor R_L (defined in eq 3)

$$R_L = \frac{1}{1 + bC_0} \tag{3}$$

where b is the Langmuir isotherm coefficients (L mg^{-1}), and C_0 is the initial MG concentration (mg L^{-1})[44] The value of b was found as 2.29 L mg^{-1}. The adsorption process is favorable, as the R_L values are between 0 and 1. In the present work, the values of R_L were found within the range of 0.00087−0.0069 for MG adsorption by the magnetic composite, indicating that the adsorption process was favorable. Moreover, the adsorption was almost irreversible (R_L was close to zero).[45]

Adsorption Kinetics. As shown in Figure 5b, the effect of contact time on the MG adsorption by the composite was studied for initial dye concentrations of 125, 187.5, and 250 mg L^{-1}. The adsorption capacity increased greatly in the initial stages, and equilibrium time increased with the increased initial dye concentration. These results suggested that the MG molecule was adsorbed first by the exterior surface of composite, and then the dye was mainly adsorbed by the interior surface of composite as the adsorption of the exterior surface achieved saturation.

To evaluate the kinetics mechanism of MG adsorption, kinetics data were interpreted by the pseudo-first-order model (eq 4), pseudo-second-order model (eq 5), and Elovich equation (eq 6).

$$\ln(q_e - q_t) = \ln q_e - k_1 t \tag{4}$$

$$\frac{t}{q_t} = \frac{1}{k_2 q_e^2} + \frac{t}{q_e} \tag{5}$$

$$q_t = \frac{1}{\beta}\ln(\alpha\beta) + \frac{1}{\beta}\ln(t) \tag{6}$$

where k_1 (min^{-1}) and k_2 (g mg^{-1} min^{-1}) are the rate constants of the pseudo-first-order and pseudo-second-order model, respectively; q_t (mg g^{-1}) is the amount of MG adsorbed onto the composite at time t; α (mg g^{-1} min^{-1}) is the initial adsorption rate; and β is the desorption constant (g mg^{-1}). In addition, the initial adsorption rate could be estimated from the pseudo-second-order equation as shown in the following equation:

$$h = k_2 q_e^2 \tag{7}$$

The estimated parameter values are listed in Table 4. Evidently, the pseudo-second-order model was the best for predicting the adsorption kinetics of MG onto the composite. In addition, the initial rate of adsorption (h) was improved with increasing initial MG concentration due to the increase in driving force for mass transfer.[41]

To elucidate rate-determining steps toward MG adsorption onto the composite, the intraparticle diffusion model (eq 8) was taken to estimate the equilibrium data[46]

$$q_t = k_{id} t^{1/2} + X \tag{8}$$

where k_{id} (mg g^{-1} $min^{-1/2}$) is the rate constant of the intraparticle diffusion model, and X is a constant characterizing boundary layer thickness. As shown in Figure 5c, the plots are multi-linear, and a two-step adsorption process is observed, indicating that a fast adsorption first occurred on the film layer and then intraparticle diffusion of the MG molecule started. Obviously, none of the X constants approached zero (Table S2, Supporting Information), suggesting that intraparticle diffusion may not exclusively control MG adsorption.[46]

Adsorption Thermodynamic. The adsorption thermodynamic parameters were estimated using the following equations

$$\ln Kc = \frac{-\Delta H^\circ_{ads}}{RT} + \frac{\Delta S^\circ}{R} \tag{9}$$

$$Kc = \frac{C_{Ae}}{C_e} \tag{10}$$

$$\Delta G^\circ = -RT \ln Kc \tag{11}$$

where Kc is the equilibrium constant; ΔH_{ads}° is standard enthalpy (kJ mol^{-1}); ΔS° is standard entropy (J mol^{-1} k^{-1}); ΔG° is standard free energy (kJ mol^{-1}); C_{Ae} is the equilibrium concentration of MG on the composite (mg L^{-1}); T is the temperature (K); and R is the gas constant (8.314 J/mol K). ΔH_{ads}° and ΔS° can be determined by plotting $1/T$ versus ln Kc.[23]

dx.doi.org/10.1021/sc400547y | ACS Sustainable Chem. Eng. 2014, 2, 969−977

The obtained thermodynamic parameters are summarized in Table 5. The spontaneous nature of the process was well

Table 5. Thermodynamic Parameters for MG Adsorption onto the Composite[a]

temperature (°C)	Kc	ΔG° (kJ mol^{-1})	ΔS° (J mol^{-1} k^{-1})	ΔH°_{ads} (kJ mol^{-1})	R^2
25	2.25	−2.01			
35	2.53	−2.38	72.8	19.8	0.91
45	3.73	−3.48			

[a]Reaction conditions: natural solution pH; C_0, 250.0 mg L^{-1}; composit, 500 mg L^{-1}; and contact time, 12 h.

explained by the negative values of free energy, and the positive value of enthalpy indicated that MG adsorption onto the magnetic composite was endothermic. This endothermic characteristic revealed that MG adsorption was more favorable at higher temperature, as confirmed as the q_e increased with increasing temperature. Furthermore, the value of enthalpy was less than 40 kJ mol^{-1}, indicating that MG adsorption onto the magnetic composite was mainly a physical adsorption.[38]

CONCLUSIONS

A novel and high-performance magnetic carbon composite was successfully synthesized from waste hydrochar in two steps using available low-cost chemicals. The prepared samples were analyzed using BET surface area, VSM, SEM/EDX, TEM, XRD, FT-IR, Raman, and XPS techniques. The prepared magnetic carbon composite showed high potential for the removal of MG and could be facilely attracted from the aqueous solution by an external magnet. In addition, the effect of solution conditions on MG adsorption was dependent on the MG initial concentration. The present study indicated that waste hydrochar is a promising material for preparation of the high-performance magnetic composite. It is also expected that the as-prepared magnetic carbon composite would be widely used for pollutants removal from wastewater. In addition, it will open a potential strategy for the further utilization of HTL solid residues of biomass wastes.

ASSOCIATED CONTENT

Supporting Information

Information as mentioned in text. This material is available free of charge via the Internet at http://pubs.acs.org.

AUTHOR INFORMATION

Corresponding Author

*Tel/Fax: +86-21-65642297. E-mail: zhangsc@fudan.edu.cn.

Notes

The authors declare no competing financial interest.

ACKNOWLEDGMENTS

The authors are thankful for financial support from the Jinlvyuan Green Engineering Co. Ltd. and the Shanghai Science and Technology Committee. The authors also thank the anonymous reviewers for fruitful suggestions.

REFERENCES

(1) Liu, Z.; Zhang, F. S. Removal of copper (II) and phenol from aqueous solution using porous carbons derived from hydrothermal chars. *Desalination* **2011**, *267*, 101−106.

(2) Li, C.; Yang, X.; Zhang, Z.; Zhou, D.; Zhang, L.; Zhang, S.; Chen, J. Hydrothermal liquefaction of desert shrub *Salix psammophila* to high value-added chemicals and hydrochar with recycled processing water. *BioResources* **2013**, *8*, 2981−2997.

(3) Zhou, D.; Zhang, L.; Zhang, S.; Fu, H.; Chen, J. Hydrothermal liquefaction of macroalgae enteromorpha prolifera to bio-oil. *Energ. Fuel.* **2010**, *24*, 4054−4061.

(4) Zhou, D.; Zhang, S.; Fu, H.; Chen, J. Liquefaction of macroalgae *Enteromorpha prolifera* in sub-/supercritical alcohols: Direct production of ester compounds. *Energ. Fuel.* **2012**, *26*, 2342−2351.

(5) Pham, M.; Schideman, L.; Scott, J.; Rajagopalan, N.; Plewa, M. J. Chemical and biological characterization of wastewater generated from hydrothermal liquefaction of Spirulina. *Environ. Sci. Technol.* **2013**, *47*, 2131−2138.

(6) Xu, Q.; Qian, Q.; Quek, A.; Ai, N.; Zeng, G.; Wang, J. Hydrothermal carbonization of macroalgae and the effects of experimental parameters on the properties of hydrochars. *ACS Sustainable Chem. Eng.* **2013**, *1*, 1092−1101.

(7) Sevilla, M.; Fuertes, A.; Mokaya, R. High density hydrogen storage in superactivated carbons from hydrothermally carbonized renewable organic materials. *Energy Environ. Sci.* **2011**, *4*, 1400−1410.

(8) Wang, H.; Ma, L.; Cao, K.; Geng, J.; Liu, J.; Song, Q.; Yang, X.; Li, S. Selective solid-phase extraction of uranium by salicylideneimine-functionalized hydrothermal carbon. *J. Hazard. Mater.* **2012**, *229*, 321−330.

(9) Sun, K.; Ro, K.; Guo, M.; Novak, J.; Mashayekhi, H.; Xing, B. Sorption of bisphenol A, 17α-ethinyl estradiol and phenanthrene on thermally and hydrothermally produced biochars. *Bioresour. Technol.* **2011**, *102*, 5757−5763.

(10) Titirici, M. M.; White, R. J.; Falco, C.; Sevilla, M. Black perspectives for a green future: hydrothermal carbons for environment protection and energy storage. *Energy Environ. Sci.* **2012**, *5*, 6796−6822.

(11) Joo, J. B.; Kim, Y. J.; Kim, W.; Kim, P.; Yi, J. Simple synthesis of graphitic porous carbon by hydrothermal method for use as a catalyst support in methanol electro-oxidation. *Catal. Commun.* **2008**, *10*, 267−271.

(12) Falco, C.; Marco-Lozar, J.; Salinas-Torres, D.; Morallón, E.; Cazorla-Amorós, D.; Titirici, M.; Lozano Castello, D. Tailoring the porosity of chemically activated hydrothermal carbons: influence of the precursor and hydrothermal carbonization temperature. *Carbon* **2013**, *62*, 346−355.

(13) Hayashi, J. i.; Horikawa, T.; Takeda, I.; Muroyama, K.; Nasir Ani, F. Preparing activated carbon from various nutshells by chemical activation with K_2CO_3. *Carbon* **2002**, *40*, 2381−2386.

(14) Ai, L.; Huang, H.; Chen, Z.; Wei, X.; Jiang, J. Activated carbon/$CoFe_2O_4$ composites: Facile synthesis, magnetic performance and their potential application for the removal of malachite green from water. *Chem. Eng. J.* **2010**, *156*, 243−249.

(15) Cheng, Z.; Gao, Z.; Ma, W. Preparation of magnetic Fe_3O_4 particles modified sawdust as the adsorbent to remove strontium ions. *Chem. Eng. J.* **2012**, *209*, 451−457.

(16) Gao, H.; Zhao, S.; Cheng, X.; Wang, X.; Zheng, L. Removal of anionic azo dyes from aqueous solution using magnetic polymer multi-wall carbon nanotube nanocomposite as adsorbent. *Chem. Eng. J.* **2013**, *223*, 84−90.

(17) Rahman, I.; Saad, B.; Shaidan, S.; Sya Rizal, E. Adsorption characteristics of malachite green on activated carbon derived from rice husks produced by chemical-thermal process. *Bioresour. Technol.* **2005**, *96*, 1578−1583.

(18) Oliveira, L. C.; Rios, R. V.; Fabris, J. D.; Garg, V.; Sapag, K.; Lago, R. M. Activated carbon/iron oxide magnetic composites for the adsorption of contaminants in water. *Carbon* **2002**, *40*, 2177−2183.

(19) Liu, P.; Liu, W. J.; Jiang, H.; Chen, J. J.; Li, W. W.; Yu, H. Q. Modification of bio-char derived from fast pyrolysis of biomass and its application in removal of tetracycline from aqueous solution. *Bioresour. Technol.* **2012**, *121*, 235−240.

(20) Keller, A. A.; Huang, Y. Magnetic nanoparticle adsorbents for emerging organic contaminants. *ACS Sustainable Chem. Eng.* **2013**, *1*, 731−736.
(21) Parker, H. L.; Budarin, V. L.; Clark, J. H.; Hunt, A. J. Use of starbon for the adsorption and desorption of phenols. *ACS Sustainable Chem. Eng.* **2013**, *1*, 1311−1318.
(22) Brunauer, S.; Deming, L. S.; Deming, W. E.; Teller, E. On a theory of the van der waals adsorption of gases. *J. Am. Chem. Soc.* **1940**, *62*, 1723−1732.
(23) Lin, L.; Zhai, S.-R.; Xiao, Z.-Y.; Song, Y.; An, Q.-D.; Song, X.-W. Dye adsorption of mesoporous activated carbons produced from NaOH-pretreated rice husks. *Bioresour. Technol.* **2013**, *136*, 437−443.
(24) Román, S.; Valente Nabais, J.; Ledesma, B.; González, J.; Laginhas, C.; M Titirici, M. Production of low-cost adsorbents with tunable surface chemistry by conjunction of hydrothermal carbonization and activation processes. *Microporous Mesoporous Mater.* **2013**, *165*, 127−133.
(25) Gollavelli, G.; Chang, C. C.; Ling, Y. C. Facile synthesis of smart magnetic graphene for safe drinking water: heavy metal removal and disinfection control. *ACS Sustainable Chem. Eng.* **2013**, *1*, 462−472.
(26) Qu, S.; Huang, F.; Yu, S.; Chen, G.; Kong, J. Magnetic removal of dyes from aqueous solution using multi-walled carbon nanotubes filled with Fe_2O_3 particles. *J.Hazard. Mater.* **2008**, *160*, 643−647.
(27) Zhang, M.; Gao, B.; Varnoosfaderon, S.; Hebard, A.; Yao, Y.; Inyang, M. Preparation and characterization of a novel magnetic biochar for arsenic removal. *Bioresour. Technol.* **2012**, *130*, 457−462.
(28) Mohan, D.; Sarswat, A.; Singh, V. K.; Alexandre-Franco, M.; Pittman, C. U. Development of magnetic activated carbon from almond shells for trinitrophenol removal from water. *Chem. Eng. J.* **2011**, *172*, 1111−1125.
(29) Hu, J.; Shao, D.; Chen, C.; Sheng, G.; Li, J.; Wang, X.; Nagatsu, M. Plasma-induced grafting of cyclodextrin onto multiwall carbon nanotube/iron oxides for adsorbent application. *J. Phys. Chem. B* **2010**, *114*, 6779−6785.
(30) Chandra, V.; Park, J.; Chun, Y.; Lee, J. W.; Hwang, I.-C.; Kim, K. S. Water-dispersible magnetite-reduced graphene oxide composites for arsenic removal. *ACS nano* **2010**, *4*, 3979−3986.
(31) Liu, Z.; Zhang, F. S.; Sasai, R. Arsenate removal from water using Fe_3O_4-loaded activated carbon prepared from waste biomass. *Chem. Eng. J.* **2010**, *160*, 57−62.
(32) Castro, C. S.; Guerreiro, M. C.; Gonçalves, M.; Oliveira, L. C.; Anastácio, A. S. Activated carbon/iron oxide composites for the removal of atrazine from aqueous medium. *J. Hazard. Mater.* **2009**, *164*, 609−614.
(33) Varadwaj, K.; Panigrahi, M.; Ghose, J. Effect of capping and particle size on Raman laser-induced degradation of γ-Fe_2O_3 nanoparticles. *J. Solid State Chem.* **2004**, *177*, 4286−4292.
(34) Han, Q.; Liu, Z.; Xu, Y.; Chen, Z.; Wang, T.; Zhang, H. Growth and properties of single-crystalline γ-Fe_2O_3 nanowires. *J. Phys. Chem. C* **2007**, *111*, 5034−5038.
(35) Pyrzyńska, K.; Bystrzejewski, M. Comparative study of heavy metal ions sorption onto activated carbon, carbon nanotubes, and carbon-encapsulated magnetic nanoparticles. *Colloids Surf., A* **2010**, *362*, 102−109.
(36) Bystrzejewski, M.; Pyrzyńska, K.; Huczko, A.; Lange, H. Carbon-encapsulated magnetic nanoparticles as separable and mobile sorbents of heavy metal ions from aqueous solutions. *Carbon* **2009**, *47*, 1201−1204.
(37) Behera, S. K.; Oh, S. Y.; Park, H. S. Sorption of triclosan onto activated carbon, kaolinite and montmorillonite: effects of pH, ionic strength, and humic acid. *J. Hazard. Mater.* **2010**, *179*, 684−691.
(38) Ji, L.; Wan, Y.; Zheng, S.; Zhu, D. Adsorption of tetracycline and sulfamethoxazole on crop residue-derived ashes: Implication for the relative importance of black carbon to soil sorption. *Environ. Sci. Technol.* **2011**, *45*, 5580−5586.
(39) Koelmans, A. A.; Meulman, B.; Meijer, T.; Jonker, M. T. Attenuation of polychlorinated biphenyl sorption to charcoal by humic acids. *Environ. Sci. Technol.* **2009**, *43*, 736−742.
(40) Giles, C.; MacEwan, T.; Nakhwa, S.; Smith, D. 786. Studies in adsorption. Part XI. A system of classification of solution adsorption isotherms, and its use in diagnosis of adsorption mechanisms and in measurement of specific surface areas of solids. *J. Chem. Soc. (Resumed)* **1960**, 3973−3993.
(41) Hameed, B.; El-Khaiary, M. Equilibrium, kinetics and mechanism of malachite green adsorption on activated carbon prepared from bamboo by K_2CO_3 activation and subsequent gasification with CO_2. *J. Hazard. Mater.* **2008**, *157*, 344−351.
(42) Jalil, A.; Triwahyono, S.; Yaakob, M.; Azmi, Z.; Sapawe, N.; Kamarudin, N.; Setiabudi, H.; Jaafar, N.; Sidik, S.; Adam, S. Utilization of bivalve shell-treated *Zea mays* L.(maize) husk leaf as a low-cost biosorbent for enhanced adsorption of malachite green. *Bioresour. Technol.* **2012**, *120*, 1621−1625.
(43) Tian, Y.; Liu, P.; Wang, X.; Lin, H. Adsorption of malachite green from aqueous solutions onto ordered mesoporous carbons. *Chem. Eng. J.* **2011**, *171*, 1263−1269.
(44) Önal, Y.; Akmil-Başar, C.; Sarıcı-Özdemir, Ç. Investigation kinetics mechanisms of adsorption malachite green onto activated carbon. *J. Hazard. Mater.* **2007**, *146*, 194−203.
(45) Feng, Y.; Yang, F.; Wang, Y.; Ma, L.; Wu, Y.; Kerr, P. G.; Yang, L. Basic dye adsorption onto an agro-based waste material-sesame hull (*Sesamum indicum L.*). *Bioresour. Technol.* **2011**, *102*, 10280−10285.
(46) Chen, Y.; Zhai, S.-R.; Liu, N.; Song, Y.; An, Q.-D.; Song, X.-W. Dye removal of activated carbons prepared from NaOH-pretreated rice husks by low-temperature solution-processed carbonization and H_3PO_4 activation. *Bioresour. Technol.* **2013**, *144*, 401−409.